

Directional locking in deterministic lateral displacement microfluidic separation systems

Sumedh R. Risbud

Chemical and Biomolecular Engineering, Johns Hopkins University

German Drazer

*Mechanical and Aerospace Engineering,
Rutgers, the State University of New Jersey*

Abstract

We analyze the trajectory of suspended spherical particles moving through a square array of obstacles, in the deterministic limit and at zero Reynolds number. We show that, in the dilute approximation of widely separated obstacles, the average motion of the particles is equivalent to the trajectory followed by a point particle moving through an array of obstacles with an effective radius. The effective radius accounts for the hydrodynamic as well as short-range repulsive non-hydrodynamic interactions between the suspended particles and the obstacles and is equal to the critical offset at which particle trajectories become irreversible. Using this equivalent system we demonstrate the presence of directional locking in the trajectory of the particles and derive an inequality that accurately describes the *Devil's staircase* type of structure observed in the migration angle as a function of the forcing direction. Finally, we use these results to determine the optimum resolution in the fractionation of binary mixtures using deterministic lateral displacement separation microfluidic systems.

I. INTRODUCTION

One of the essential unit operations in micro-total-analysis-systems (μ TAS) is the separation of species for downstream analysis. Early microfluidic separation strategies involved miniaturization of different macroscopic separation methods, e.g., size exclusion [1] and hydrodynamic chromatography [2]. However, current micro-fabrication techniques enable design and fabrication of precisely controlled micro-structures to act as separation media, in contrast with the random micro-structure common in conventional separation media. For example, ‘entropic trapping’ a channel with alternating thick and thin regions was used to separate DNA molecules by size based on the time they spend in the entropic traps (thick regions) [3]. In ‘pinched flow fractionation’, species entering a constriction and exiting into a sudden expansion experience a lateral displacement from their trajectories that is a function of their size [4]. ‘Deterministic lateral displacement’ (DLD) employs a periodic array of solid obstacles, through which species of different sizes migrate in different spatial directions in the presence of the same driving force [5]. This effect can also be achieved with a periodic array of optical traps (soft potentials instead of solid obstacles, [6]). Although DLD systems have been studied extensively [5, 7–10], the understanding of the underlying mechanism is presented only heuristically, and lacks a theoretical framework for their analysis.

We have performed numerous detailed computational and experimental studies of DLD-like systems [11–16] – where the experiments include microfluidic as well as macroscopic platforms at low Reynolds number – and have established that *directional locking* dictates the particle trajectories in such systems. In this work, we focus on the mechanism underlying separations in the DLD systems. Specifically, we present a theoretical analysis of DLD systems, involving the motion of a particle of arbitrary radius in a square array of obstacles of circular cross-section. We assume a ‘dilute limit’ for the obstacles, such that the inter-obstacle spacing is sufficiently large and a particle interacts with a single obstacle at a time. The field driving the particle (either a constant force, or a flow field) is assumed to be at an arbitrary angle (henceforth, forcing angle) with respect to the principal lattice directions of the square array. We assume negligible particle as well as fluid inertia, and infinite Péclet number (non-Brownian particles, deterministic trajectories). We show that, under the dilute approximation, the particle-obstacle interaction can be replaced by a point particle moving

in straight lines past an obstacle with an effective radius equal to the critical offset. The critical offset is the offset at which particle-obstacles collisions become irreversible and can be interpreted as a length-scale that characterizes the effect of short-range repulsive non-hydrodynamic interactions between the particles and the obstacles. (Previous work presents a detailed discussion of the critical offset, both computationally [12] as well as theoretically [17]). Using this equivalent representation of the system under the dilute approximation, the problem of calculating the particle trajectories reduces to simple geometric manipulations. We derive a periodicity criterion for particle trajectories in terms of the design parameters of the system, namely, the critical offset, the forcing angle, and the inter-obstacle spacing in the square array. The periodicity criterion yields the experimentally and computationally observed directional locking behavior. Further, we show that the same framework can be used to uncover size-based spatial band-pass filtering of particles through the array, such that particles of a certain intermediate size migrate with an average migration angle larger than that corresponding to smaller as well as larger particles.

The article is organized as follows: in §II we introduce the system under consideration, the system variables, and the dilute approximation. We also explain the model for short-range repulsive non-hydrodynamic interactions leading to the definition of the critical parameter b_c , and establish an abstract model for the particle-obstacle pair. In §III, we use the abstract model to derive a periodicity condition for particle trajectories. We apply the periodicity condition to derive expressions for the simplest locking directions in §III B 1 and §III B 2. In §IV, we use the periodicity condition corresponding to particles exhibiting the simplest directional locking behavior, and comment on the resolution of separation between such particles.

II. SYSTEM DESCRIPTION, ASSUMPTIONS AND ABSTRACTIONS

Figure 1 depicts the system under investigation. We consider a suspended spherical particle of radius a negotiating a square array of obstacles with circular cross section of radius b , under the action of a driving field \mathbf{F} (either a constant force, or a uniform flow away from the lattice). The field is oriented at an angle θ with respect to one of the principal axes of the array (say, the X -axis as shown in the figure). The lattice spacing is ℓ . The domain of the ‘forcing angle’ is restricted to $\theta \in [0, \frac{\pi}{4}]$, since the system possesses a reflection

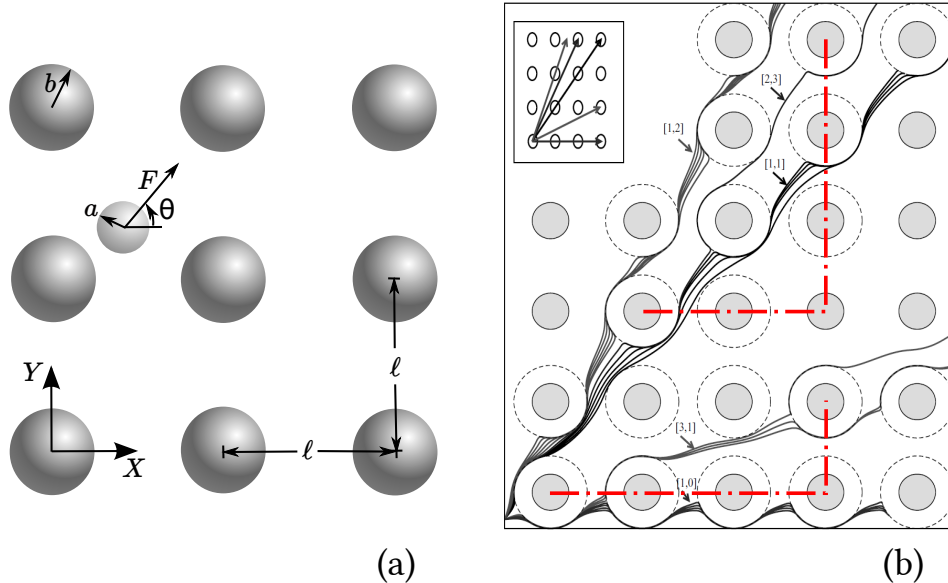


FIG. 1. (a) A spherical particle of radius a negotiating a portion of a square array of obstacles of circular cross-section with radius b [adapted from [12]]: the length of a unit-cell is ℓ , the driving field \mathbf{F} , oriented at an angle θ as shown, drives the particle through the array. The principal lattice-directions are indicated with Cartesian axes X and Y . (b) A few example particle trajectories exhibiting directional locking [adapted from [12]]: results of Stokesian dynamics simulations with $a = b$, $\ell = 5a$ and the range of non-hydrodynamics interactions $\epsilon = 10^{-3}$ (see §II for a discussion on non-hydrodynamic interactions). Counter-clockwise, from X -axis to Y -axis, the trajectories can be seen to be locked in directions $[1, 0]$, $[3, 1]$, $[1, 1]$, $[2, 3]$ and $[1, 2]$ (the inset shows the migration directions). The dot-dashed lines are to guide the eye and highlight $[3, 1]$ and $[2, 3]$ locking directions.

symmetry in the $X = Y$ line.

We work in the ‘Stokes regime’, i.e., we neglect fluid inertia (vanishingly small Reynolds number) and particle inertia (vanishingly small Stokes number). We consider the deterministic limit (infinitely large Péclet number, non-Brownian limit). Further, in DLD micro-devices, the enclosing walls perpendicular to the Z -axis (i.e., walls parallel to the plane of the paper) screen the hydrodynamic interactions between the particle and distant obstacles. Therefore, we assume that the lattice spacing ℓ is sufficiently larger than the Z -spacing between the walls, such that, to a good approximation we can consider the interaction between the particle and only the closest obstacle (figure 2, dilute approximation). Figure 2 depicts the variables of the problem; the incoming and outgoing offsets are denoted by b_{in} and b_{out} , respectively. The dimensionless minimum surface-to-surface separation attained by the particle from the obstacle is denoted by ξ_{min} in the figure. The functional relationship between

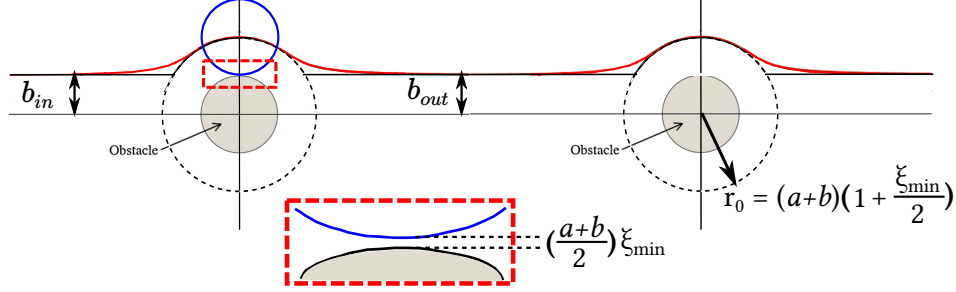


FIG. 2. A schematic depicting the variables of the problem, b_{in} , b_{out} and ξ_{min} . The dashed circular region (excluded volume) has radius $r_0 = (a+b)(1 + \frac{\xi_{min}}{2})$. The schematic qualitatively shows the ‘dilute approximation’, wherein two consecutive obstacles are sufficiently separated that considering only the interaction between the particle and its closest obstacle is a good approximation. Note that the particle trajectory is seen to attain the asymptotic value of b_{out} in between consecutive collisions.

b_{in} and ξ_{min} explicitly incorporates the hydrodynamic mobility of the particle around the fixed obstacle, thereby taking into consideration the hydrodynamic interactions [17].

Apart from the hydrodynamic interactions between the particle and the obstacle that arise from their finite size, we also take into account the effect of short-range repulsive non-hydrodynamic interactions such as solid-solid contact due to surface roughness, electrostatic repulsion, steric repulsion, etc. A simple and effective model for these non-hydrodynamic interactions is to treat them as leading to a hard-wall potential with a given dimensionless range ϵ , such that it creates a hard shell around the obstacle and the particle surface cannot approach the obstacle surface closer than ϵ [12, 18–28]. We have shown elsewhere that the presence of such non-hydrodynamic repulsion leads to the occurrence of a critical offset b_c [17, 29]. This can be further elaborated with the aid of figure 3(a). As shown, the particle trajectories can be categorized as follows (from top to bottom): (a) the trajectories for which $\xi_{min} > \epsilon$. In this case, the particle motion is unaffected by the presence of the non-hydrodynamic interactions, (b) the trajectory that corresponds to $\xi_{min} = \epsilon$. In this case, the particle ‘grazes’ the obstacle and defines the *critical trajectory*, and (c) the trajectories that would correspond to $\xi_{min} < \epsilon$ in the absence of non-hydrodynamic interactions. However, in this case, the particles are forced to circumnavigate the obstacle by maintaining a constant separation equal to ϵ on the approaching side due to the hard-core potential. The last group of trajectories collapse onto the critical trajectory downstream of the obstacle, breaking their fore-aft symmetry. Thus, the critical trajectory (of type (b) described above) defines

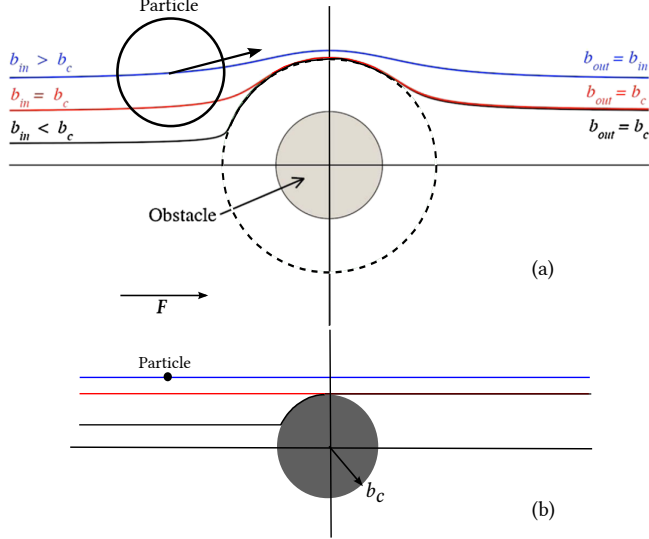


FIG. 3. (a)[Adapted from [11]] Three kinds of particle trajectories in the presence of short-range repulsive non-hydrodynamic interactions. (b) Depiction of the equivalent system in which a point-particle traverses past an obstacle of radius b_c (effective radius). The outgoing part of the trajectories with $b_{in} < b_c$ is tangent to the obstacle in the equivalent system.

the critical offset as $b_{in} = b_c$, such that the corresponding minimum separation is the range of the non-hydrodynamic interactions (i.e., $\xi_{min,c} = \epsilon$). Therefore, in the presence of short-range repulsive non-hydrodynamic interactions, the relationship between b_{in} and ξ_{min} is equivalent to the relationship between the critical offset b_c and the range of the interactions ϵ [11–13, 17, 29, 30].

Using the hard-wall model for the non-hydrodynamic interactions combined with the dilute assumption, we can thus replace the physical particle-obstacle system with an equivalent abstract system shown in figure 3(b). The obstacle radius b can be replaced by b_c and the particle can be reduced to a point particle. As shown, since the particle trajectories with incoming impact parameter $b_{in} > b_c$ remain fore-aft symmetric, one can replace them with straight lines uninfluenced by the obstacle. The trajectories with $b_{in} < b_c$ (that would intersect the new, abstract obstacle), get laterally displaced by $(b_c - b_{in})$, and continue as tangents to the obstacle parallel to the forcing direction. It is interesting to note that both the hydrodynamic as well as non-hydrodynamic interactions are incorporated in the single parameter b_c .

III. MATHEMATICAL DESCRIPTION OF DIRECTIONAL LOCKING

The defining feature of deterministic lateral displacement is directional locking of particle trajectories (see figure 1(b)). In a square array of obstacles (e.g., DLD devices), the particle follows a periodic trajectory with a periodicity of (say) p lattice units in X -direction and q lattice units in Y -direction for a range of values of θ , and some integers p & q . In such a case, the trajectory is said to be locked in the $[p, q]$ direction for that range of values of θ . The migration angle α is defined by,

$$\tan \alpha = \frac{q}{p}.$$

Equipped with the abstraction of the particle-obstacle pair described in the previous section, we now consider a square array of such obstacles with radius b_c , separated by the lattice spacing ℓ . Figure 4 shows a schematic of the equivalent system with straight-line trajectories between two successive particle-obstacle collisions that occur p lattice units apart in X -direction and q lattice units apart in Y -direction, thereby representing a $[p, q]$ -periodic trajectory. The figure shows two coordinate systems, the XY -system with its axes parallel to the principal axes of the lattice as well as the xy -system with x -axis parallel to the direction of the driving field \mathbf{F} . Since we have a point-particle traversing in a straight line parallel to the direction of the driving field, it is evident that a particle-obstacle interaction (a ‘collision’) is possible only if the particle trajectory intersects the obstacle, i.e., only if the distance d to the obstacle center from the trajectory is less than the obstacle radius. Note that, as shown in figure 4, d is the same as the initial offset b_{in} for the corresponding obstacle. It is evident that there are only two kinds of collisions with respect to the sign of the y -coordinate of the point of collision, *top* ($y > 0$) and *bottom* ($y < 0$) ones. Therefore, a given periodic trajectory, can exhibit periodicity in exactly three distinct modes: (a) all successive collisions satisfy $y > 0$ (*top-top collisions*, figure 4(a)), (b) all successive collisions satisfy $y < 0$ (*bottom-bottom collisions*, figure 4(b)), or (c) collisions alternately satisfy $y > 0$ and $y < 0$ (*top-bottom-top collisions* or equivalently, *bottom-top-bottom collisions* figure 4(c))

As shown in figure 4, we choose an arbitrary obstacle, which has undergone a collision, as the origin of the XY -system. In the case of top-top and bottom-bottom collisions (figure 4(a) and (b)), we assume that the period is p in X -direction, and q in Y -direction, for

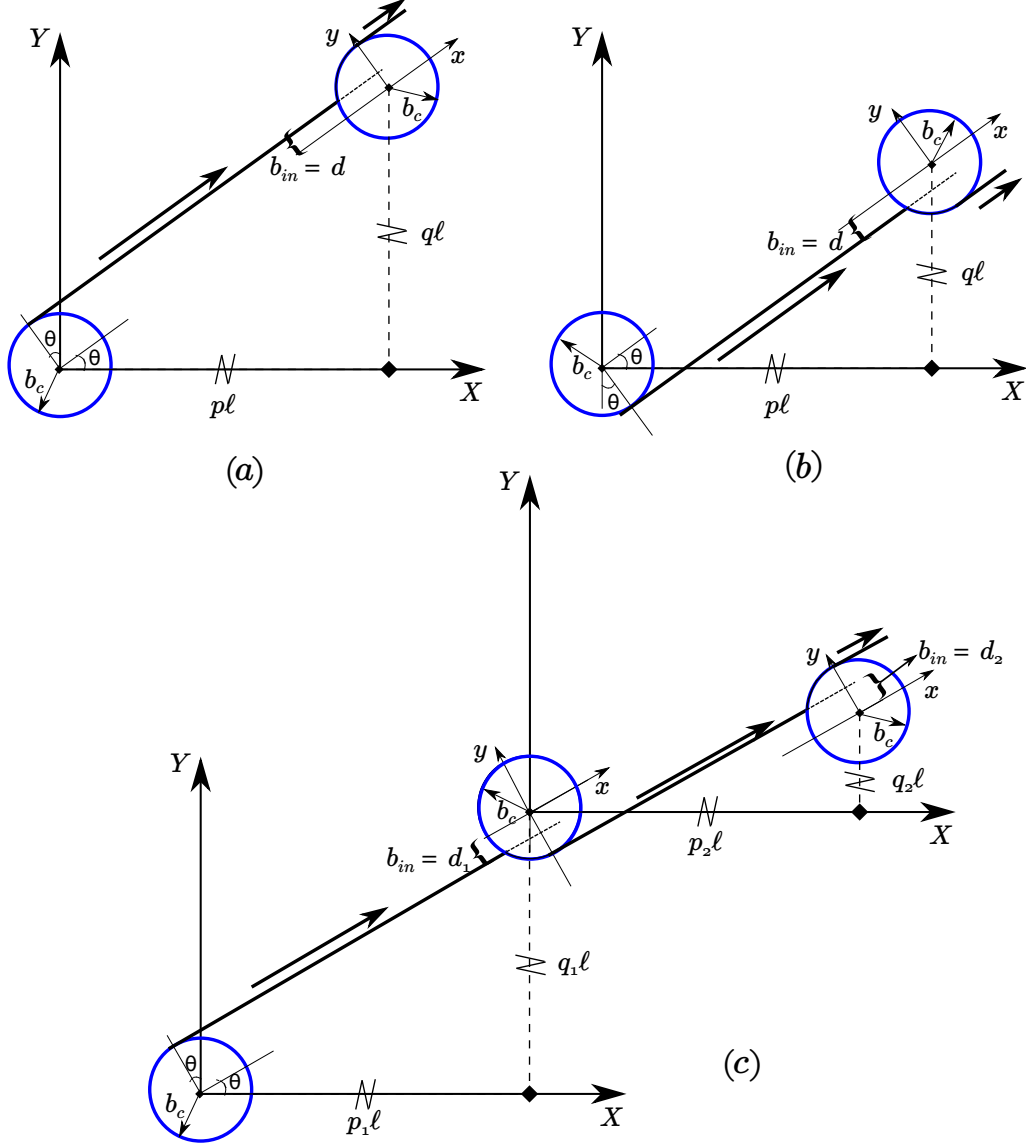


FIG. 4. Schematic depicting three possibilities leading to periodic trajectories (see text). In (a) and (b), the trajectories repeat after p obstacles along X -axis and q obstacles along Y -axis. In (c), the period along X -axis is $(p_1 + p_2)$ and that along Y -axis is $(q_1 + q_2)$.

some integers p & q . Hence the coordinates of the center of the next obstacle are $(p\ell, q\ell)$ in figures 4(a) and (b). In the case of periodic trajectories arising from top-bottom-top (equivalently, bottom-top-bottom) collisions (figure 4(c)), we assume that p_1 and p_2 are the alternate periods in X -direction, while q_1 and q_2 are the periods in Y -direction, again, for some integers p_1, p_2, q_1 & q_2 .

A. The periodicity-condition

For a top-top collision, the equation of the trajectory in the XY -system is,

$$Y = X \tan \theta + b_c \sec \theta.$$

Since the center of the next obstacle, $(p\ell, q\ell)$, lies in the lower half-plane of the trajectory, it satisfies $q\ell < p\ell \tan \theta + b_c \sec \theta$. Therefore, the normal distance between the obstacle center and the trajectory in the case of top-top collisions is,

$$d_{TT} = \frac{p\ell \tan \theta - q\ell + b_c \sec \theta}{\sqrt{1 + \tan^2 \theta}} = p\ell \sin \theta - q\ell \cos \theta + b_c \quad (1)$$

For a top-top collision, in the xy -system centered on the second obstacle, the initial offset must satisfy $0 \leq b_{in} = d_{TT} < b_c$. Therefore, (1) yields, $0 < q\ell \cos \theta - p\ell \sin \theta \leq b_c$. This inequality can be rephrased as,

$$0 < \sin(\alpha - \theta) \leq \frac{b_c}{s\ell}, \quad (2)$$

where, $s([p, q]) = \sqrt{p^2 + q^2}$.

A similar procedure for bottom-bottom collisions dictates that the trajectory is described by

$$Y = X \tan \theta - b_c \sec \theta.$$

The obstacle center $(p\ell, q\ell)$, lies in the upper half-plane of the trajectory satisfying $q\ell > p\ell \tan \theta - b_c \sec \theta$. Therefore,

$$d_{BB} = \frac{q\ell - p\ell \tan \theta + b_c \sec \theta}{\sqrt{1 + \tan^2 \theta}} = q\ell \cos \theta - p\ell \sin \theta + b_c \quad (3)$$

The bounds on b_{in} in xy -system dictate, $-b_c < b_{in} = -d_{BB} \leq 0$. Therefore, (3) becomes, $-b_c \leq q\ell \cos \theta - p\ell \sin \theta < 0$. The latter can be rearranged to,

$$0 < \sin(\theta - \alpha) \leq \frac{b_c}{s\ell}, \quad (4)$$

where, $s([p, q]) = \sqrt{p^2 + q^2}$.

For top-bottom-top collisions leading to periodicity, we can similarly arrive at $-b_c < p_1\ell \sin \theta - q_1\ell \cos \theta + b_c \leq 0$ and $0 \leq p_2\ell \sin \theta - q_2\ell \cos \theta - b_c < b_c$ for the first (top-bottom) and the second (bottom-top) collisions, respectively. Since these always occur successively in a periodic trajectory, we can add the two inequalities to yield,

$$-b_c \leq (q_1 + q_2)\ell \cos \theta - (p_1 + p_2)\ell \sin \theta \leq b_c.$$

Using the total periodicity $[p, q] = [p_1 + p_2, q_1 + q_2]$ and s as defined earlier, the above inequality can be rearranged to take a form similar to (2) or (4):

$$-\frac{b_c}{s\ell} \leq \sin(\alpha - \theta) \leq \frac{b_c}{s\ell} \quad \equiv \quad -\frac{b_c}{s\ell} \leq \sin(\theta - \alpha) \leq \frac{b_c}{s\ell}.$$

In the above double-inequalities, only one side becomes relevant depending on the relative magnitudes of θ and α . If $\theta < \alpha$ we have $\sin(\alpha - \theta) > 0$, and inequality (2) is relevant, whereas in the case of $\theta > \alpha$, the inequality (4) is the appropriate choice.

Thus, (2) and (4) together describe the periodic behavior of the particle trajectories in the lattice. Both can be combined into a single inequality as,

$$|\sin(\alpha - \theta)| \leq \frac{b_c}{s\ell}. \quad (5)$$

We observe that the values of θ satisfying the inequality (5) are symmetric about $\theta = \alpha$. Which means, if $\tilde{\theta}_c$ and θ_c satisfy the *equalities* corresponding to (2) and (4), respectively, then

$$\alpha = \frac{\tilde{\theta}_c + \theta_c}{2}.$$

Further, note that (2) and (4) are *necessary conditions* for periodicity of a trajectory in a strict mathematical sense, but they are not sufficient conditions. Which means, *if* a trajectory is known to exhibit $[p, q]$ -locking, *then* the pair $[p, q]$ must satisfy (2) or (4) depending upon the relative magnitudes of α and θ . Conversely, there may exist many integer pairs $[p, q]$ which satisfy (2) or (4), for a given forcing angle θ and parameters b_c and ℓ . However, physically, the trajectory would become periodic after a collision with the obstacle closest to the one at the origin, i.e., *only if* the pair $[p, q]$ is the closest possible pair to the origin $[0, 0]$ satisfying the inequalities. Thus, the converse problem of finding the periodicity $[p, q]$

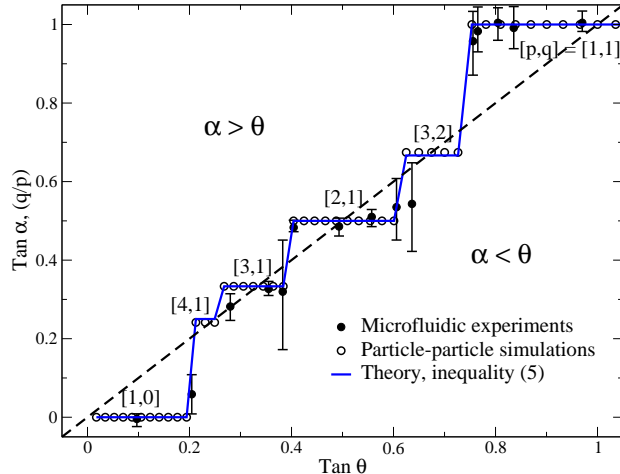


FIG. 5. Migration direction ($\tan \alpha$) versus forcing direction ($\tan \theta$) portraying devil’s staircase-like structure representing directional locking. The empty circles represent individual particle-particle simulations under the dilute approximation, the line represents the solution of (5), $[p, q]$, such that the integer pair $[p, q]$ is the closest integer pair to $[0, 0]$. The filled circles with error bars correspond to the data from microfluidic experiments [16]. The dashed line represents the 1-1-line dividing the plane in the regions with $\alpha > \theta$ (the region above the line) and $\alpha < \theta$ (the region below the line) as shown. The inequality (2) is satisfied along the solid line forming the staircase in the region above the 1-1-line, whereas the inequality (4) is satisfied along the solid line forming the staircase below the 1-1-line.

lies in the domain of mixed integer minimization problems, stated as: minimize $\sqrt{p^2 + q^2}$ for integers p and q subject to the constraints $p > 0$, $q \geq 0$, and the inequalities (2) and (4).

In figure 5, we show an excellent agreement between the migration angles ($\tan \alpha = q/p$) obtained by solving either (2) or (4) for the pairs $[p, q]$ corresponding to the smallest s ($[p, q]$) (using `Mathematica`[®]), and those obtained from trajectory calculations using particle-particle simulations under the dilute assumption [12], for different forcing angles. The same critical offset b_c is used in both cases, which corresponds to a particle of the same size as the obstacle ($a = b$) and a range of non-hydrodynamic interactions $\epsilon = 10^{-3}a$ (the inter-obstacle spacing is $\ell = 5a$). The same figure also shows an agreement between data from microfluidic experiments [16] and theory (the ratio b_c/ℓ corresponding to the experimental data shown in the figure is approximately equal to that used in theoretical calculations).

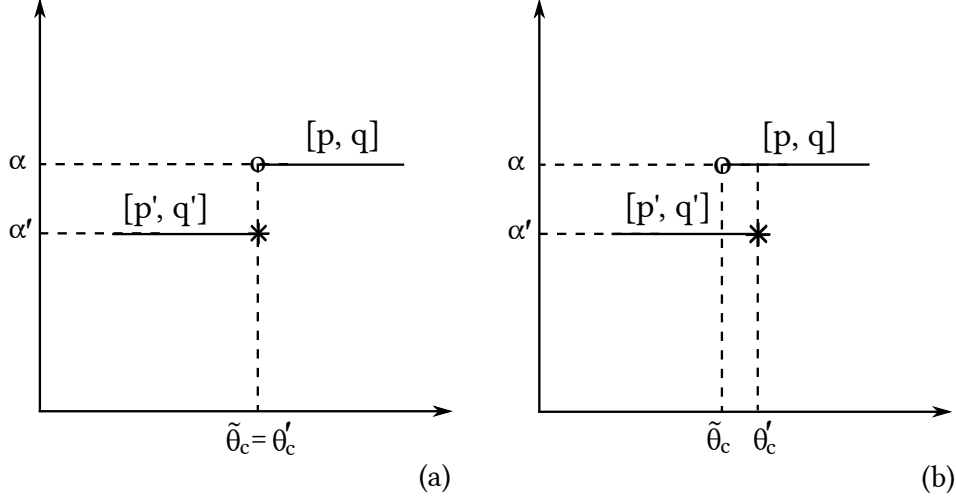


FIG. 6. Schematic showing two consecutive locking directions, $[p', q']$ and $[p, q]$. (a) There is no region in which the periodicities satisfy either of the two inequalities (2) and (4) simultaneously. (b) Both periodicities satisfy one of the two inequality simultaneously in the region of overlap. The transition angles at the end of $[p', q']$ and beginning of $[p, q]$ are denoted by θ'_c and $\tilde{\theta}_c$, respectively.

B. Transitions from and to periodicities

The transition-forcing-angles from one locked migration direction to the next as well as the migration angle itself, can be computed by treating (2) and (4) as equalities. We have noted earlier that for each periodicity $[p, q]$ corresponding to a migration angle $\tan \alpha = q/p$, two distinct transition angles $\tilde{\theta}_c$ and θ_c can be obtained from the equalities corresponding to (2) and (4), by solving $\sin(\alpha - \tilde{\theta}_c) = b_c/s\ell$ and $\sin(\theta_c - \alpha) = b_c/s\ell$, respectively. Then, consider two consecutive locking directions $[p', q']$ and $[p, q]$, with the primed direction representing the ‘lower’ step in the staircase (i.e., $\alpha' < \alpha$), as shown in schematic 6. If the periodicities do not *simultaneously* satisfy the inequalities (2) and (4), then there is no overlap between the two steps as shown in figure 6(a). Therefore, the the transition from $[p', q']$ to $[p, q]$ takes place at the end of the lower step, given by $\theta = \theta'_c$ (* point in the figure). But since there is no overlap between the steps, this has to be the angle at the beginning of the $[p, q]$ -step, given by $\theta = \tilde{\theta}_c$ (‘o’ point in the figure). Therefore, this is the case when both critical angles are equal ($\tilde{\theta}_c = \theta'_c$), and either equality corresponding to (2) or (4) gives the same result. An example of such a transition is seen in figure 5 from $[3, 1]$ -periodicity to $[2, 1]$ -periodicity. Although $s([2, 1]) = \sqrt{5} < s([3, 1]) = \sqrt{10}$, there is no forcing direction θ for which both inequalities are satisfied, and there is no overlap between the corresponding steps. If there is an overlap between the steps as shown in figure 6(b), the two inequalities are satisfied for the forcing

directions θ in the overlap region. Then in the region of overlap, the step with a smaller s is realised, thus satisfying the physical requirement that the trajectory becomes periodic with the shortest period. An example of this type of transition is that from $[4, 1]$ -periodicity to $[3, 1]$ -periodicity, shown in figure 5. In this case, since $s([3, 1]) = \sqrt{10} < s([4, 1]) = \sqrt{17}$, the transition occurs before $\theta = \theta_{c,[4,1]}$ (the end of $[4, 1]$ -step). Therefore, in the case of an overlap between the steps,

- (a) if $s < s'$, then the transition occurs at the beginning of $[p, q]$ (equality in (2)) at the ‘o’-point (in figure 6(b))
- (b) else/otherwise, the transition occurs at the end of $[p', q']$ at the ‘*’-point in the figure.

We apply the above argument to the transitions from- and to- $[1, 0]$ and $[1, 1]$ -directions, respectively the simplest possible locking directions.

- The transition from $[1, 0]$: Since $[1, 0]$ gives the smallest possible s -value ($s = 1$), the transition always occurs at the end of $[1, 0]$ -step, i.e., using the equality in (4),

$$\sin(\theta_F - 0) = \sin \theta_F = \frac{b_c}{\ell}, \quad (6)$$

where θ_F is defined as the first transition angle.

- The transition to $[1, 1]$: The final locking direction $[1, 1]$ gives the second smallest possible s -value ($s = \sqrt{2}$). Therefore, the transition to $[1, 1]$ -direction always occurs at the beginning of the $[1, 1]$ -step, i.e., using the equality in (2),

$$\sin\left(\frac{\pi}{4} - \theta_L\right) = \frac{b_c}{\sqrt{2}\ell}, \quad (7)$$

where, θ_L is the last transition angle.

The only exception to (7) is when there is a direct transition from $[1, 0]$ to $[1, 1]$, which is the case of a one-step staircase. In this case, $s = 1 < s = 2$, the transition takes place at $\theta = \theta_F$ (the end of the $[1, 0]$ -step), which may or may not be the same as $\theta = \theta_L$ (the beginning of the $[1, 1]$ -step).

1. *The first locking direction after [1, 0]*

If the locking direction after the first transition is $[p_F, q_F]$, then

$$|q_F \cos \theta_F - p_F \sin \theta_F| \leq \frac{b_c}{\ell}.$$

However, from (6), $\sin \theta_F = b_c/\ell$. Also, increasing θ counter-clockwise from X - to Y -axis, the first transition should be from a locking direction along the zeroth row of obstacles along X -axis (i.e., $[1, 0]$) to the first row of obstacles along X -axis (i.e., $[p, 1]$ for some integer p). Therefore, $q_F = 1$ (see figure 1(b)). Thus, $|\cot \theta_F - p_F| \leq 1$. Since p_F is an integer, we get,

$$p_F = \lfloor \cot \theta_F \rfloor \quad \dots \quad \lfloor \cdot \rfloor \equiv \text{floor function} \quad (8)$$

Thus, the locked direction after the first transition is $\tan \alpha = q_F/p_F = 1/\lfloor \cot \theta_F \rfloor$, where θ_F is given by (6) above.

2. *The last locking direction before [1, 1]*

If the locking direction before the final transition is $[p_L, q_L]$, then

$$|q_L \cos \theta - p_L \sin \theta| \leq \frac{b_c}{\ell}.$$

From (7), $\cos \theta_L - \sin \theta_L = b_c/\ell$. Further, increasing θ counter-clockwise from X - to Y -axis, the last transition from $[p_L, q_L]$ to $[q_L, q_L]$ (i.e., $[1, 1]$) should satisfy $p_L = q_L + 1$. Thus, the above inequality becomes, $\left| \left(\frac{\sin \theta_L}{\cos \theta_L - \sin \theta_L} \right) - q_L \right| \leq 1$. Since q_L is an integer,

$$q_L = \left\lfloor \frac{\sin \theta_L}{\cos \theta_L - \sin \theta_L} \right\rfloor = \left\lfloor \frac{\tan \theta_L}{1 - \tan \theta_L} \right\rfloor. \quad (9)$$

Therefore, the locked direction before the final transition to $[1, 1]$ is given as

$$\tan \alpha = q_L/p_L = \frac{\left\lfloor \frac{\tan \theta_L}{1 - \tan \theta_L} \right\rfloor}{\left\lfloor \frac{\tan \theta_L}{1 - \tan \theta_L} \right\rfloor + 1},$$

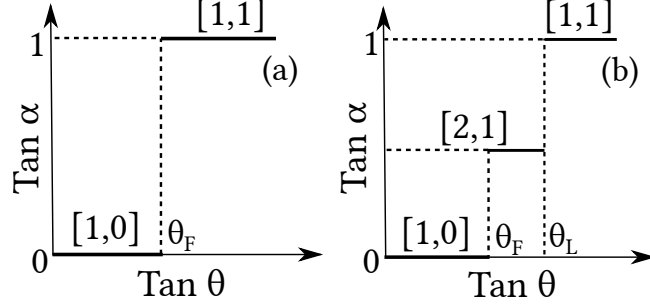


FIG. 7. (a) 1-step staircase with transition $[1,0] \mapsto [1,1]$ at θ_F (b) 2-step staircase $[1,0] \mapsto [2,1] \mapsto [1,1]$ with transitions at θ_F and θ_L .

where, θ_L is the solution of (7). We note again, that the only exception to the calculation leading to (9) is the case when the transition to $[1,1]$ occurs from $[1,0]$. In this case, the transition occurs at corresponding θ_F instead of θ_L .

IV. DESIGN RULES AND SEPARATION RESOLUTION IN DLD FOR SIMPLE STAIRCASE STRUCTURES

We first derive the constraints on the ratio b_c/ℓ for a particle to exhibit exactly one transition (figure 7(a)) and exactly two transitions (figure 7(b)), based on (5) and the discussion in §III. We have shown in §III B that the first transition angle is given by $\sin \theta_F = b_c/\ell$ corresponding to the transition from the $[1,0]$ locking direction. Further, we have noted earlier that θ_L from (9) is not necessarily equal to θ_F , since the transition to $[1,1]$ from $[1,0]$ is an exception. Therefore, applying the constraint (2) for θ_F we get,

$$\sin\left(\frac{\pi}{4} - \theta_F\right) \leq \frac{b_c}{\ell\sqrt{2}} \Rightarrow \tan \theta_F \leq \frac{1}{2}, \quad (10)$$

and,

$$\frac{b_c}{\ell} \geq \frac{1}{\sqrt{5}} \dots \left(\text{using } \sin \theta_F = \frac{b_c}{\ell}\right). \quad (11)$$

Thus, for a fixed particle radius a , obstacles of size b , and a range ϵ of non-hydrodynamic interactions (i.e., for a fixed b_c), a square lattice with $\ell \geq \sqrt{5}b_c$ can be constructed in which the particle exhibits a 1-step staircase structure.

In the case of a 2-step staircase (figure 7(b)), the locking direction after the first transition from $[1,0]$ is $[2,1]$, which is the same as the locking direction before the final transition to

[1, 1]. Using §§III B 1, III B 2,

$$\tan \alpha = \frac{1}{2} = \frac{1}{[\cot \theta_F]} = \frac{\left\lfloor \frac{\tan \theta_L}{1 - \tan \theta_L} \right\rfloor}{\left\lfloor \frac{\tan \theta_L}{1 - \tan \theta_L} \right\rfloor + 1} \quad \& \quad \sin \theta_F = b_c/\ell$$

The first set of equations above yields, $[\cot \theta_F] = 2$ and $\left\lfloor \frac{\tan \theta_L}{1 - \tan \theta_L} \right\rfloor = 1$. Thus, using $\sin \theta_F = b_c/\ell$, we obtain,

$$\frac{1}{3} < \tan \theta_F \leq \frac{1}{2} \leq \tan \theta_L < \frac{2}{3} \quad (12)$$

$$\frac{1}{\sqrt{10}} < \frac{b_c}{\ell} \leq \frac{1}{\sqrt{5}}. \quad (13)$$

Thus, if a square lattice satisfies (13) for a particle of radius a , a critical parameter b_c (a function of a , b and ϵ) and unit cell ℓ , then the particle exhibits locking with a 2-step staircase structure with the corresponding two transition angles satisfying (12).

A. Design constraints and separation resolution in DLD

In pairwise size-based separation, two particles of different sizes, say a and a' (and perhaps different length-scales corresponding to the range of non-hydrodynamic interactions, say ϵ and ϵ') exhibit two distinct critical parameters, viz.- b_c and b'_c . Separation is possible at forcing angles such that the migration directions $\tan \alpha = q/p$ and $\tan \alpha' = q'/p'$ are distinct. Further, a larger difference between the migration directions is synonymous with a higher resolution. Thus, a simple design strategy is to maximize $|\alpha - \alpha'|$.

By rearranging (5) as,

$$\left| \sqrt{q^2 + p^2} \sin(\alpha - \theta) \right| \approx \left| \sqrt{q^2 + p^2} (\alpha - \theta) \right| \leq \frac{b_c}{\ell}, \quad (14)$$

where, the last inequality results from the small angle approximation $\sin(\alpha - \theta) \approx (\alpha - \theta)$ since $0 < \alpha, \theta \leq \pi/4$. Similarly, a good approximation for $|\alpha - \alpha'|$ can be obtained by combining (14) for both particles a and a' ,

$$|\alpha - \alpha'| \leq \frac{b_c}{\left(\sqrt{p^2 + q^2}\right) \ell} + \frac{b'_c}{\left(\sqrt{p'^2 + q'^2}\right) \ell} \quad (15)$$

As an immediate consequence of (14), we note that the largest difference between the migration direction and the forcing direction (i.e., $|\tan \alpha - \tan \theta| \approx |\alpha - \theta|$) occurs before the first transition from $\alpha = 0$ (locking $\equiv [1, 0]$ and when $p^2 + q^2 = 1$), and it is always equal to $|\alpha - \theta| = \theta \lesssim b_c/\ell$. Furthermore, along with (15), we infer that the largest separation resolution between two species can be obtained when one of the species has undergone its first transition, while the other is still locked in $[1, 0]$ direction (for example, $\theta_F < \theta < \theta'_F$). This observation supports our earlier experimental inference that, it is the most beneficial strategy to set the forcing angle between the first transitions (θ_F and θ'_F) of the two species undergoing separation [11, 15, 16]. The inequality, i.e., expression (15) not only gives an upper bound on the resolution, but also gives design constraints on the obstacle radius b and the lattice spacing ℓ through the ratio b_c/ℓ for known locking directions ($[p, q]$ and $[p', q']$), a fixed forcing angle θ and known radii of particles (a and a'). In the following, we illustrate this result for particles with simple staircase structures, viz.- only one transition from $[1, 0]$ to $[1, 1]$ and two transitions $[1, 0] \mapsto [2, 1] \mapsto [1, 1]$.

For a mixture of two species, both exhibiting 1-step staircases with different transitions θ_F and θ'_F satisfying (10) and (11), it is readily understood that the forcing angle needs to be between these two values if any separation is desired. The separation resolution $|\alpha - \alpha'|$ is always $\pi/4$ in this case, since one species is always locked in $[1, 0]$ -periodicity, while the other is locked in $[1, 1]$ -periodicity for a forcing angle between θ_F and θ'_F .

In the case of a mixture of a species exhibiting a 1-step staircase (say, for particles of radius a') and another species exhibiting a 2-step staircase (say, for particles of radius a), then (10) and (12) permit only one possible scenario depicted in (figure 8(a)). After appropriate algebra corresponding to this case, we get,

$$\frac{1}{3} < \tan \theta_F \leq \frac{1}{2} \leq \tan \theta'_F \leq \tan \theta_L < \frac{2}{3}.$$

Similarly, for a mixture of particles exhibiting a 2-step staircase, (6), (7) and (12) permit only two cases depicted in figures 8(b) and 8(c), which correspond to the two cases $b_c > b'_c$ or $b_c < b'_c$, respectively. Again, applying these constraints we get,

$$\frac{1}{3} < \tan \theta'_F < \tan \theta_F \leq \frac{1}{2} < \tan \theta_L < \tan \theta'_L < \frac{2}{3},$$

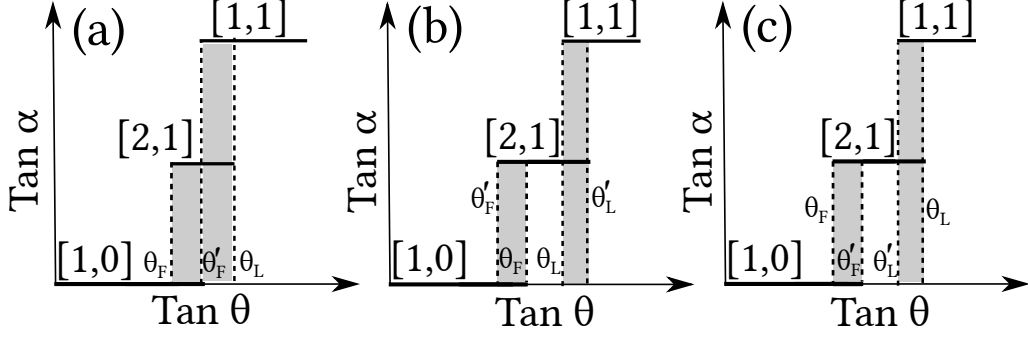


FIG. 8. Three combinations of the simplest staircase structures possible: (a) one particle exhibits 1-step staircase, the other exhibits 2-step staircase, with the former transition lying between the two transitions of the latter, (b) and (c) both particles exhibit 2-step staircase structures. The shaded areas represent the ranges of forcing angle θ in which separation between the two species is possible.

or

$$\frac{1}{3} < \tan \theta_F < \tan \theta'_F \leq \frac{1}{2} < \tan \theta'_L < \tan \theta_L < \frac{2}{3}.$$

In terms of separation, it is evident from the figure that separation between primed and non-primed species is possible only if the forcing angle satisfies

- (i) $\theta \in [\theta_F, \theta'_F] \cup [\theta'_F, \theta_L]$ corresponding to figure 8(a),
- (ii) $\theta \in [\theta'_F, \theta_F] \cup [\theta_L, \theta'_L]$ for figure 8(b), and
- (iii) $\theta \in [\theta_F, \theta'_F] \cup [\theta'_L, \theta_L]$ in the case of figure 8(c).

Further, the figure also indicates that $(\pi/4 - \arctan(1/2))$ and $\arctan(1/2)$ are the only two separation resolutions ($|\alpha - \alpha'|$) corresponding to these cases.

Thus, the maximum separation resolution between species corresponding to the three cases shown in figure 8 is $\arctan(1/2) \approx 26.56^\circ$ since it is greater in magnitude than $[\pi/4 - \arctan(1/2)]$, and it occurs if $\theta \in [\theta_F, \theta'_F]$ for figure 8(a), $\theta \in [\theta'_F, \theta_F]$ for figure 8(b) and $\theta \in [\theta_F, \theta'_F]$ for figure 8(c). As highlighted in the context of (15), this conclusion is consistent with our experimental observation, that the forcing angle between the first transition angles of the species to be separated, achieves the best resolution [11, 15, 16].

V. SUMMARY

In summary, we have presented a theoretical analysis of the directional locking phenomenon exhibited by particles navigating through a square array of obstacles, in the limit of negligible particle and fluid inertia. In the dilute limit for the array (i.e., a sparse array), interactions between a single obstacle and a particle are sufficient for trajectory analysis. Coupled with the dilute assumption, we have used a critical parameter (incorporating both hydrodynamic as well as short-range repulsive non-hydrodynamic particle-obstacle interactions) to replace the physical particle-obstacle system with its kinematically equivalent abstraction. Within the abstract model, the particle is replaced by a point-particle, while the obstacle radius is scaled to be equal to the critical parameter. Due to the model, a simple geometric analysis suffices to derive the periodicity condition, both necessary and sufficient for the particle trajectory. The periodicity condition directly leads to the devil's-staircase-like behavior of the migration direction as a function of the forcing direction. Further, using the periodicity condition, we have computed the design constraints on the ratio of the critical parameter to the lattice spacing of the square array, and commented on the resolution of deterministic separations, when the particle exhibits simple staircase structures.

This work was partially supported by the National Science Foundation Grant Nos. CBET-0731032 and CBET-1339087.

-
- [1] G. Chirica, J. Lachmann, and J. Chan. Size exclusion chromatography of microliter volumes for on-line use in low-pressure microfluidic systems. *Analytical Chemistry*, 78(15):5362–5368, 2006. doi:10.1021/ac060258t.
 - [2] M. T. Blom, E. Chmela, R. E. Oosterbroek, R. Tijssen, and A. van den Berg. On-chip hydrodynamic chromatography separation and detection of nanoparticles and biomolecules. *Analytical Chemistry*, 75(24):6761–6768, 2003.
 - [3] J. Han and H. G. Craighead. Separation of long DNA molecules in a microfabricated entropic trap array. *Science*, 288(5468):1026–1029, 2000.
 - [4] M. Yamada, M. Nakashima, and M. Seki. Pinched flow fractionation: continuous size separation of particles utilizing a laminar flow profile in a pinched microchannel. *Anal. Chem.*, 76(18):5465–5471, 2004.

- [5] L. R. Huang, E. C. Cox, R. H. Austin, and J. C. Sturm. Continuous Particle Separation Through Deterministic Lateral Displacement. *Science*, 304(5673):987–990, 2004.
- [6] M. P. MacDonald, G. C. Spalding, and K. Dholakia. Microfluidic sorting in an optical lattice. *Nature*, 426:421–424, 2003.
- [7] D. W. Inglis, K. J. Morton, J. A. Davis, T. J. Zieziulewicz, D. A. Lawrence, R. H. Austin, and J. C. Sturm. Microfluidic device for label-free measurement of platelet activation. *Lab Chip*, 8(6):925–931, 2008.
- [8] P. T. Korda, G. C. Spalding, and D. G. Grier. Evolution of a colloidal critical state in an optical pinning potential landscape. *Phys. Rev. B*, 66:024504, 2002.
- [9] A. M. Lacasta, J. M. Sancho, A. H. Romero, and K. Lindenberg. Sorting on periodic surfaces. *Phys. Rev. Lett.*, 94(16):160601, 2005.
- [10] A. Gopinathan and D. G. Grier. Statistically locked-in transport through periodic potential landscapes. *Phys. rev. lett.*, 92(13):130602, 2004.
- [11] M. Balvin, E. Sohn, T. Iracki, G. Drazer, and J. Frechette. Directional locking and the role of irreversible interactions in deterministic hydrodynamics separations in microfluidic devices. *Phys. Rev. Lett.*, 103:078301, 2009.
- [12] J. Frechette and G. Drazer. Directional locking and deterministic separation in periodic arrays. *J. Fluid Mech.*, 627:379–401, 2009.
- [13] J. Herrmann, M. Karweit, and G. Drazer. Separation of suspended particles in microfluidic systems by directional locking in periodic fields. *Phys. Rev. E*, 79(6):061404, 2009.
- [14] J. Koplik and G. Drazer. Nanoscale simulations of directional locking. *Phys. Fluids*, 22(5):052005, 2010.
- [15] T. Bowman, Frechette J., and Drazer G. Force driven separation of drops by deterministic lateral displacement. *Lab Chip*, 12:2903–2908, 2012.
- [16] R. Devendra and G. Drazer. Force driven deterministic lateral displacement for particle separation in microfluidic devices. *Anal. Chem.*, 84:10621, 2012.
- [17] S. R. Risbud and G. Drazer. Trajectory and distribution of non-brownian suspended particles moving past a fixed spherical or cylindrical obstacle. *J. Fluid Mech.*, 714:213–237, 2013.
- [18] R. H. Davis. Effects of surface-roughness on a sphere sedimenting through a dilute suspension of neutrally buoyant spheres. *Phys. Fluids*, 4(12):2607–2619, December 1992.
- [19] F. R. da Cunha and E. J. Hinch. Shear-induced dispersion in a dilute suspension of rough

- spheres. *J. Fluid Mech.*, 309:211–223, 1996.
- [20] I. Rampall, J. R. Smart, and D. T. Leighton. The influence of surface roughness on the particle-pair distribution function of dilute suspensions of non-colloidal spheres in simple shear flow. *J. Fluid Mech.*, 339:1–24, 1997.
- [21] J. F. Brady and J. F. Morris. Microstructure of strongly sheared suspensions and its impact on rheology and diffusion. *J. Fluid Mech.*, 348(1):103–139, 1997.
- [22] H. J. Wilson and R. H. Davis. The viscosity of a dilute suspension of rough spheres. *J. Fluid Mech.*, 421:339–367, 2000.
- [23] J. Bergenholtz, J. F. Brady, and M. Vucic. The non-Newtonian rheology of dilute colloidal suspensions. *J. Fluid Mech.*, 456:239–275, 2002.
- [24] G. Drazer, J. Koplik, B. Khusid, and A. Acrivos. Deterministic and stochastic behaviour of non-Brownian spheres in sheared suspensions. *J. Fluid Mech.*, 460:307–335, 2002.
- [25] R. H. Davis, Y. Zhao, K. P. Galvin, and H. J. Wilson. Solid-solid contacts due to surface roughness and their effects on suspension behaviour. *Phil. Trans. R. Soc. A*, 361(1806):871–894, 2003.
- [26] G. Drazer, J. Koplik, B. Khusid, and A. Acrivos. Microstructure and velocity fluctuations in sheared suspensions. *J. Fluid Mech.*, 511:237–263, 2004.
- [27] M. S. Ingber, S. Feng, A. L. Graham, and H. Brenner. The analysis of self-diffusion and migration of rough spheres in nonlinear shear flow using a traction-corrected boundary element method. *J. Fluid Mech.*, 598:267–292, 2008.
- [28] F. Blanc, F. Peters, and E. Lemaire. Experimental signature of the pair trajectories of rough spheres in the shear-induced microstructure in noncolloidal suspensions. *Phys. Rev. Lett.*, 107:208302, 2011.
- [29] S. R. Risbud, M. Luo, J. Frechette, and G. Drazer. Analysis of the trajectory of a sphere moving through a geometric constriction. *Phys. Fluids*, 25:062001, 2013.
- [30] M. Luo, F. Sweeney, S. R. Risbud, G. Drazer, and J. Frechette. Irreversibility and pinching in deterministic particle separation. *Appl. Phys. Lett.*, 99(6):064102, 2011.